Pergamon

Bioorganic & Medicinal Chemistry 10 (2002) 2543–2552

BIOORGANIC & MEDICINAL CHEMISTRY

Fluorescent Somatostatin Receptor Probes for the Intraoperative Detection of Tumor Tissue with Long-Wavelength Visible Light

Walter Mier,[a,*] Barbro Beijer,[a,†] Keith Graham[a] and William E. Hull[b]

[a]*Department of Nuclear Medicine, University of Heidelberg, INF 400, D-69120 Heidelberg, Germany*
[b]*Central Spectroscopy Department, German Cancer Research Center, INF 280, D-69120 Heidelberg, Germany*

Received 7 November 2001; accepted 27 March 2002

Abstract—Targeted fluorescent dyes are of substantial value for the intraoperative delineation of primary tumors and metastatic lesions. For this purpose long-wavelength red light ($\lambda = 550$–650 nm) offers advantages because of good tissue penetration and direct visibility. Since somatostatin receptors (SSTR) are overexpressed in a number of tumors, a series of potentially tumor-selective peptide–dye conjugates were synthesized by solid-phase peptide synthesis (SPPS). The octapeptides octreotate, Tyr^3-octreotate and Tyr^3-octreotide were employed and exhibited high affinity for somatostatin receptors (SSTR). The fluorescent dyes rhodamine 101, sulforhodamine B acid chloride, sulforhodamine 101 or rhodamine B isothiocyanate were conjugated either directly or via spacers, for example the peptidase-labile pentapeptide sequence Ala-Leu-Ala-Leu-Ala. The conjugates were completely assembled on the solid support: Fmoc-SPPS, cyclization via a disulfide linkage, N-terminal attachment of a spacer, and linkage to the fluorescent dye. An in vitro competition assay revealed that the conjugates bind to SSTRs with IC_{50} values between 0.7 and 89 nM. The conjugates were generally stable to hydrolysis at pH 7–8 in buffer or serum. However, the rhodamine 101 conjugates revealed a loss of absorption at alkaline pH due to conversion to a neutral spirolactam form, as characterized by NMR. © 2002 Published by Elsevier Science Ltd.

Introduction

The best postoperative prognostic factors related to overall survival can usually be achieved by radical dissection of tumors. This includes removal of the lymph nodes and the surrounding, possibly infiltrated tissue.[1] Improved visual discrimination of malignant versus benign tissues can reduce the extent of dissection required. This visual discrimination enables the in situ diagnosis of several malignancies such as gliomas, bladder tumors, pancreatic lesions, as well as head and neck tumors. In cutaneous areas, endoscopically accessible areas, and in intraoperative situations, fluorescent contrast enhancement markers can be used for this purpose. Significant differences are found in the autofluorescence emission properties of tumor versus normal tissues. These differences can be increased by systemic administration of the heme precursor 5-aminolevulinic acid (ALA). Application of ALA results in the preferential accumulation of protoporphyrin IX in neoplastic tissues.[2,3] These techniques are limited because of the low tumor specificity of the currently used dyes (hematoporphyrin and phthalocyanine).

Extensive research effort has been made in the quest for organ- and tissue-specific contrast agents. Targeting strategies have improved the selective accumulation of fluorescent dyes by coupling of the dyes to antibodies directed against tumor-associated antigens.[4] Recently, it has been shown that enhanced expression of the green fluorescent protein (GFP) gene results in an impressive detectability of metastatic sites.[5] Upon illumination with UV light, chelate complexes of the lanthanide terbium emit fluorescence with an enormous Stokes shift of 280 nm. These complexes are preferentially taken up into adenocarcinomas.[6] Abnormalities of the vascular system of tumor tissue facilitate the extravasation of macromolecules. Consequently, increased uptake of fluorescent dye-labeled cationic polymers has been shown in an orthotopic rat prostate cancer model.[7] Transferrin and albumin have been used as macromolecular carriers of indotricarbocyanine dyes.[8] Clinical applications of conjugates of 5-aminofluorescein with albumin have been successfuly demonstrated, for example for the intraoperative detection of malignant gliomas.[9] Dyes conjugated to membrane-impermeable high-molecular-weight polymers have been injected into indivi-

*Corresponding author. Tel.: +49-6221-56-7727; e-mail: walter_mier@med.uni-heidelberg.de
†Current address: febit ag, Käfertaler Straße 190, 68167 Mannheim, Germany.

0968-0896/02/$ - see front matter © 2002 Published by Elsevier Science Ltd.
PII: S0968-0896(02)00114-1

dual cells, and the fate of these cells has been followed using fluorescence.[10] Several papers report on conjugates that are cleaved by enzymes which are overexpressed in tumors.[11] Many of these developments are designed for near-infrared (NIR) reflectance imaging detection, using dyes which fluoresce in the NIR region (750–1000 nm). This technique offers high resolution and sensitivity through the use of an amplifying CCD camera.

However, techniques for intraoperative detection and handling under direct visual control are not yet available. For this purpose dyes which emit fluorescent light in the visible range are required. Unfortunately, several tissue constituents such as the blood chromophores show autofluorescence in the visible spectrum, which impedes the use of dyes which fluoresce in the short-wavelength region ($\lambda < 550$). Since tissue penetration increases with increasing excitation and emission wavelengths, the optical 'window' between 550 and 650 nm offers the possibility of deep penetration, low background, and ease of visualization.

Somatostatin receptors (SSTR) have been found in a variety of neuroendocrine tumors, such as carcinoids and paragangliomas, as well as in most pancreatic endocrine tumors and breast tumors. Somatostatin receptor scintigraphy with radionuclide-labeled somatostatin analogues is a sensitive and specific technique for visualizing tumors which could not be detected by conventional imaging techniques. Imaging of somatostatin receptors using ^{111}In-diethylenetriaminepentaacetic-acid-octreotide[12] has proven to be helpful in the differentiation and follow-up of meningiomas, neurinomas or neurofibromas and their metastases.[13] Recently, [^{68}Ga]1,4,7,10-tetraazacyclododecane-*N*,*N*′,*N*″,*N*‴-tetraacetic-acid-D-Phe^1-Tyr^3-octreotide has been used to localize neuroendocrine tumors with high resolution.[14] These SSTR-specific peptides can be used to target macromolecules or cytotoxic drugs. Consequently, such peptides can act as specific carriers for fluorescent dyes which absorb and emit visible light. As a first step for assessing the feasibility of this approach, we have developed synthesis protocols for preparing fluorescent probes derived from SSTR-specific peptides. We report here on the synthesis, stability, and receptor affinity of long-wavelength fluorescent dyes conjugated with potent SSTR-specific peptides.

Results

Synthesis strategy and chemistry

Structure–activity relationship studies have shown that the N-terminal phenylalanine of the cyclic octapeptides octreotide and octreotate (Fig. 1) can tolerate *N*-substitution with minimal effect on SSTR affinity and internalization rate. Therefore, we chose to attach fluorescent dyes at this position via a suitable spacer. The Tyr^3 modification of the peptide moiety was used for several conjugates in view of the favorable pharmacokinetic behavior of tyrosine-modified octreotide derivatives and for the purpose of obtaining an iodinatable tracer. Figure 1 shows the structures of the peptides used and compound **14** as an example for the conjugates. According to the Merrifield strategy, the peptide conjugates were synthesized manually using Fmoc-protected amino acids. The octreotate peptide H-D-Phe-Cys(Acm)-Phe-D-Trp(Boc)-Lys(Boc)-Thr(*t*-Bu)-Cys(Acm)-Thr(*t*-Bu)-OH and its Tyr^3 analogue H-D-Phe-Cys(Acm)-Tyr(*t*-Bu)-D-Trp(Boc)-Lys(Boc)-Thr(*t*-Bu)-Cys(Acm)-Thr(*t*-Bu)-OH were

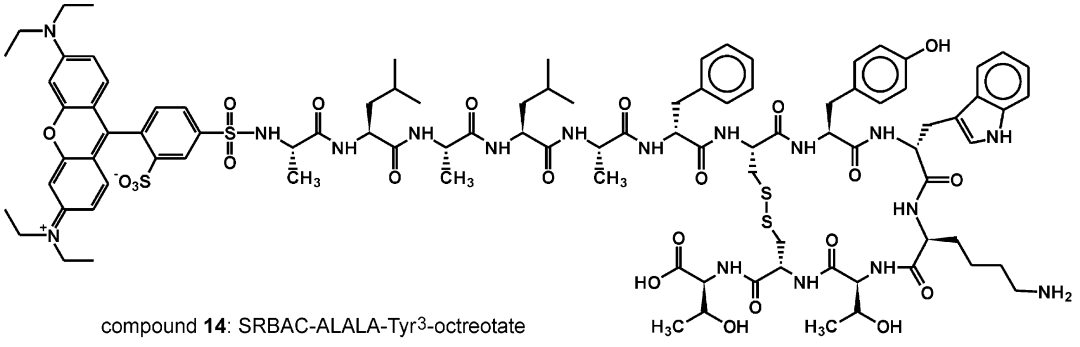

compound **14**: SRBAC-ALALA-Tyr3-octreotate

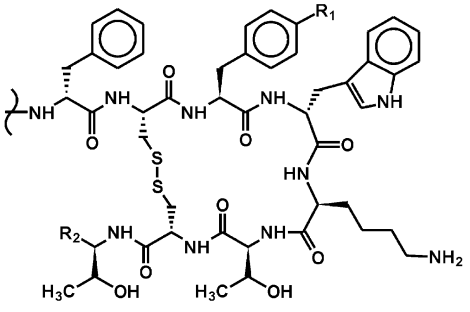

Peptide moieties:

octreotide: R_1 = -H, R_2 = -CH_2OH
octreotate: R_1 = -H, R_2 = -COOH
Tyr3-octreotate: R_1 = -OH, R_2 = -COOH

Figure 1. Chemical structures of the cyclic peptides (somatostatin analogues) used to prepare fluorescent peptide–dye conjugates. As an example, the complete structure for conjugate **14** (SRBAC-ALALA-Tyr^3-octreotate) is shown.

synthesized on Wang resin. The Tyr^3-octreotide peptide precursor H-D-Phe-Cys(Acm)-Tyr(*t*-Bu)-D-Trp(Boc)-Lys (Boc)-Thr(*t*-Bu)-Cys(Acm)-Thr(ol)-terephthal-acetal was prepared on Rink amide resin.

Attempts to cyclize the peptide using $Tl(TFA)_3$ on the solid support *after* conjugation with the fluorescent moiety failed because of the lability of rhodamine derivatives to oxidation. An alternative method with air oxidation is time-consuming and may also cause damage to the rhodamine dyes. It was found that oxidation of the resin-bound peptide with $Tl(TFA)_3$ did not influence subsequent couplings of amino acids, the 6-aminohexanoic spacer, or the rhodamine dyes. Consequently, conjugation with a spacer and a fluorescent dye could be performed after cyclization of the peptide on the solid support. As an example, the solid-phase synthesis of compound **14** is shown schematically in Figure 2. The peptide moiety and the dye molecule were coupled either directly via various spacer molecules: lysine, 6-aminohexanoic acid (Ahx), or the pentapeptide Ala-Leu-Ala-Leu-Ala (ALALA). The ALALA pentapeptide has been shown to be susceptible to hydrolysis by hydrolases in the lysosomal compartment of cells.[15] SSTR-specific compounds are known to be taken up by receptor-mediated endocytosis into lysosomal compartments.[16] Consequently, intracellular trapping of the cleaved dye may be achieved by inclusion of a hydrolase-labile linker. Therefore, the lysosomal hydrolase-sensitive linker ALALA was incorporated into several of the conjugates.[17] The structures of the rhodamine dyes and spacer molecules used are shown in Figure 3. Rhodamine 101 (R101) was coupled via its carboxy group, analogous to the coupling of amino acids, using 1*H*-benzotriazol-1-yl) (HBTU) and diisopropylethylamine (DIPEA). The activated rhodamine dyes sulforhodamine B acid chloride (SRBAC), sulforhodamine 101 acid chloride (SR101AC) and rhodamine B isothiocyanate (RBITC) were coupled using DIPEA as a base. The conjugates were deprotected with TFA-containing water, with phenol and TIS as scavengers, and the products were isolated in high yields by HPLC. The homogeneity of the final products was estimated by analytical RP-HPLC (see Experimental). The purity of all conjugates was determined to be $>95\%$ on the basis of the absorption at $\lambda = 254$ nm. A typical HPLC-chromatogram of **16** is shown in Figure 4. For all of the conjugates the synthesis was initially confirmed by MALDI-TOF-MS at low resolution. Since the mass difference between the cyclic (disulfide) and open-chain peptide is only 2 mass units, it was necessary to confirm the results using MALDI-TOF or electrospray (ESI) mass spectrometry with higher resolution and an absolute accuracy of ca. ± 0.5 mass units. Table 1 summarizes the mass spectrometry results and other physical properties for the synthesized compounds **1**–**16**.

Stability of the conjugates to hydrolysis

The stability of the fluorescent peptide–dye conjugates to hydrolysis or enzymic degradation was investigated in Soerensen buffer (pH 7.4) and in rat serum at 37 °C. Here, a striking property of the amide-linked rhodamine 101 (R1O1) conjugates **1**–**6**, namely, a pH-dependent equilibrium between an open amide and a spirolactam form of the R101 benzamide moiety (see below), made it difficult to assess by HPLC the stability of these compounds to hydrolysis. In contrast, the stability of conjugates with a sulfonamide or thiourea dye linkage could be assessed by HPLC. Compound **9** was slowly degraded in buffer or serum with a half-life of 18 h, while **7** was unstable

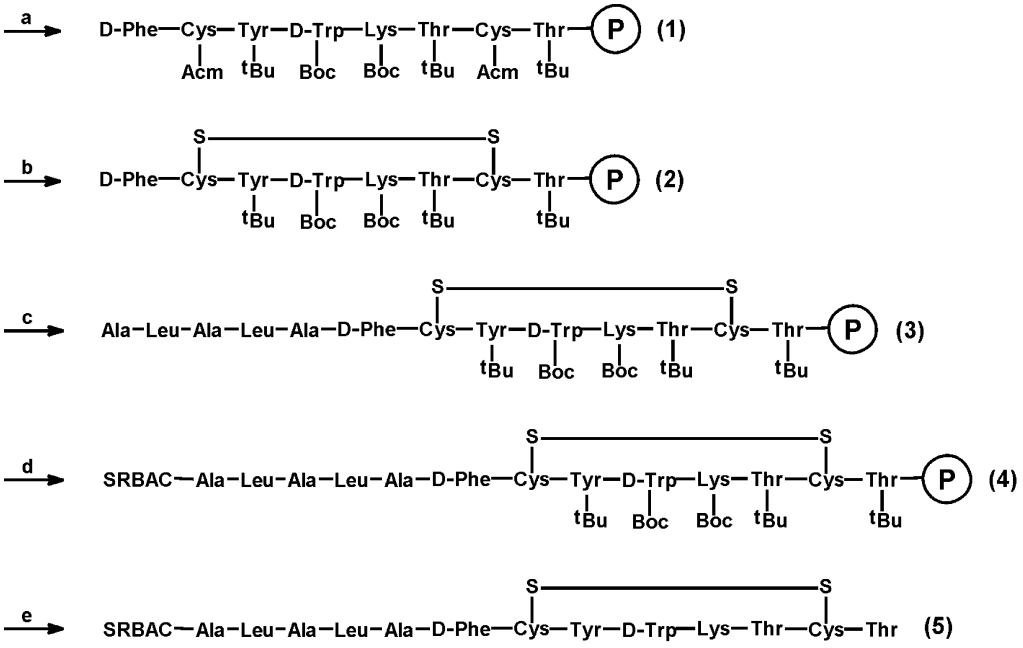

Figure 2. Schematic representation of the solid-phase synthesis protocol used to prepare fluorescent peptide–dye conjugates (example: SRBAC-ALALA-Tyr^3-octreotate **14**). Key: (a) beginning with the resin-bound C-terminal amino acid, stepwise N-terminal elongation, (b) cyclization using $Tl(TFA)_3$, (c) stepwise N-terminal elongation to form the spacer ALALA, (d) attachment of the dye SRBAC after preactivation with DIPEA, (e) cleavage of the conjugate from the resin using TFA, H_2O, phenol, and TIS.

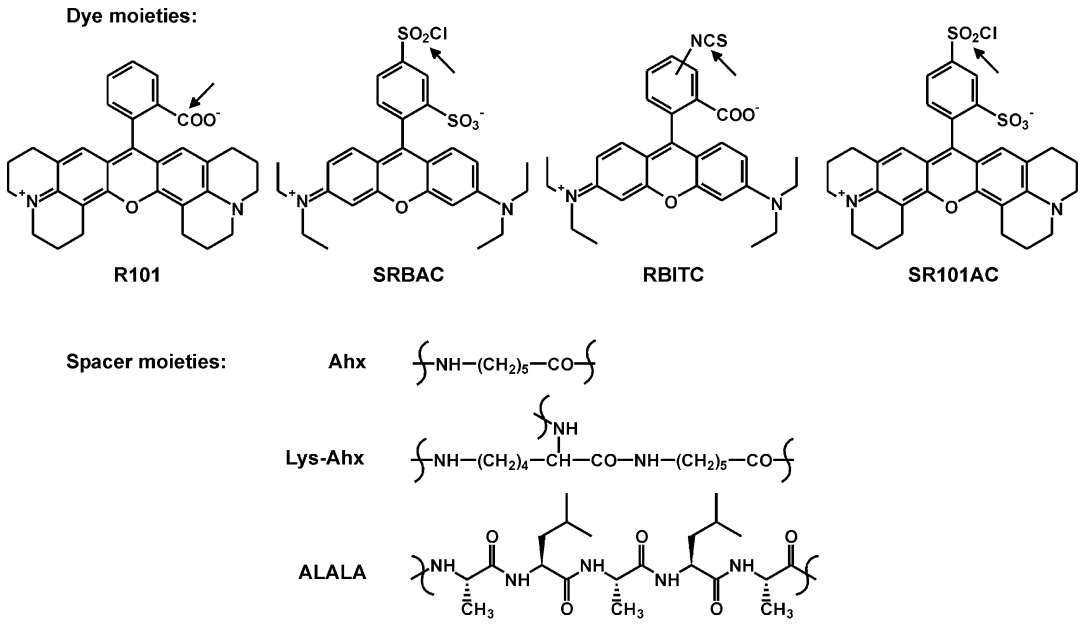

Figure 3. Chemical structures of the spacer moieties and dye molecules used to prepare conjugates containing the rhodamine fluorophore in the form rhodamine 101 (R101), sulforhodamine B acid chloride (SRBAC), rhodamine B isothiocyanate (RBITC), or sulforhodamine 101 acid chloride (SR101AC). The C-terminus of a chosen spacer was attached to a peptide, and the N-terminus was attached to a dye molecule at the site indicated by an arrow. RBITC was supplied as a mixture of isomers.

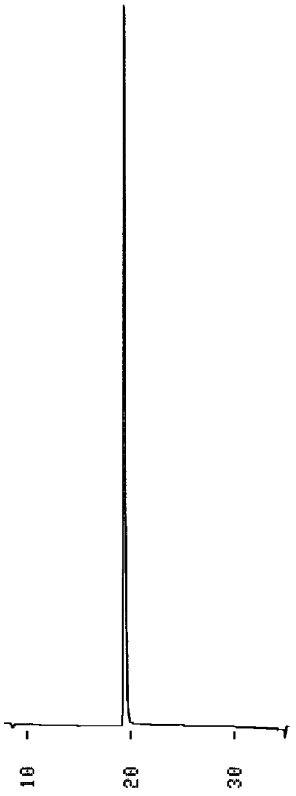

Figure 4. RP-HPLC chromatogram of the purified conjugate SR101AC-Ahx-Tyr^3-octreotate (**16**). Conditions: C_{18} column, solvent A = 0.1% TFA (v/v) in acetonitrile, solvent B = 0.1% TFA (v/v) in water; elution with a linear gradient of 5 to 95% solvent A in solvent B over 30 min.

only in serum with a half-life of 24 h. Compounds **8** and **10**–**16** were stable with no sign of decomposition after 24 h. Thus, conjugates **7**–**16**, with various peptide and spacer moieties, are relatively insensitive to hydrolysis at pH 7.4 or to enzymatic degradation in serum. Therefore, we expect that the R101 conjugates **1**–**6** are also stable to hydrolysis.

Somatostatin receptor binding

The affinities of the synthesized conjugates for the somatostatin receptor were determined as IC_{50} values for a competition assay using radiolabeled ^{125}I-Tyr^3-octreotide ($K_D = 0.08$ nM)[18] and rat cortex membranes (see Experimental). As shown in Table 1 all of the fluorescent conjugates exhibit relatively high affinity for the SSTR with IC_{50} ranging from 0.72 nM for **14** to 89 nM for **11**. For comparison, under the same assay conditions, the IC_{50} for octreotide was found to be 2.78 ± 0.17 nM. Thus, only compound **14** has an IC_{50} significantly lower than that for octreotide. Conjugates **1**, **4**, **5**, **6**, **10**, and **13** have affinities very similar to that of octreotide (IC_{50} values ranging from 2.0 to 4.3 nM), while **3**, **7**, **8**, **12**, and **16** are slightly poorer competitors (IC_{50} values: 5.5–10 nM). Finally, conjugates **2**, **9**, **11**, and **15** have significantly poorer affinity (IC_{50} values: 27–89 nM, see Discussion).

Lactam formation by rhodamine 101 conjugates

During incubation in buffer at pH 7.4, the color of the R101 conjugates **1**–**6** faded within minutes, and HPLC analysis with TFA buffer showed two peaks whose ratios depended on incubation time. The reverse effect was also observed; when the pH of a solution of conjugate **1**, for example, was shifted from 7.4 to 4.0, the UV absorption increased again (Fig. 5).

This behavior can be explained by a slow pH-dependent interconversion between the positively charged rhodamine form with benzamide moiety and a neutral spirolactam form in which the benzamide nitrogen of the

Table 1. Properties of the synthesized fluorescent peptide–dye conjugates

No.	Name (dye-linker-peptide)	Molecular formula[a]	*m/z* (pos. ion)		Ret. time[d] (min)	λ_{max} (nm) (H_2O/DMF 4:1)	IC_{50} (nM) Mean ± SD (*n*)
			Calcd[b]	Meas.[c]			
1	R101-Ahx-Tyr^3-octreotide	$C_{87}H_{106}N_{13}O_{14}S_2^+$	1620.74	1620.86	22.33	599	2.4 ± 0.4 (2)
2	R101-octreotate	$C_{81}H_{93}N_{12}O_{13}S_2^+$	1505.64	1506.11	22.63	600	58 ± 13 (2)
3	R101-ALALA-octreotate	$C_{102}H_{130}N_{17}O_{18}S_2^+$	1944.92	1944.77	24.03	597	8.6 ± 2.0 (4)
4	R101-Ahx-Tyr^3-octreotate	$C_{87}H_{104}N_{13}O_{15}S_2^+$	1634.72	1635.00	22.80	599	2.0 ± 0.6 (3)
5	R101-ALALA-Tyr^3-octreotate	$C_{102}H_{130}N_{17}O_{19}S_2^+$	1960.92	1960.71	23.54	598	4.3 ± 1.9 (3)
6	R101-Ahx-Lys(R101)-Tyr^3-octreotate	$C_{125}H_{145}N_{17}O_{18}S_2^{+2}$	2235.03	2235.79	25.71	598	2.9 ± 1.2 (2)
7	RBITC-Ahx-Tyr^3-octreotide	$C_{84}H_{106}N_{14}O_{15}S_3$	1647.72	1648.0	21.95	583	5.5 ± 0.0 (2)
8	RBITC-Ahx-Tyr^3-octreotate	$C_{84}H_{104}N_{14}O_{16}S_3$	1661.70	1661.0	21.80	583	8.2 ± 6.5 (3)
9	RBITC-ALALA-Tyr^3-octreotate	$C_{99}H_{130}N_{18}O_{20}S_3$	1987.89	1989.0	24.05	571	27 (1)
10	SRBAC-Ahx-Tyr^3-octreotide	$C_{82}H_{105}N_{13}O_{18}S_4$	1688.67	1689.41	20.21	582	3.6 ± 1.2 (2)
11	SRBAC-octreotate	$C_{76}H_{92}N_{12}O_{17}S_4$	1573.57	1573.87	21.29	583	89 ± 29 (3)
12	SRBAC-ALALA-octreotate	$C_{97}H_{129}N_{17}O_{22}S_4$	2012.85	2013.70	22.52	584	10 (1)
13	SRBAC-Ahx-Tyr^3-octreotate	$C_{82}H_{103}N_{13}O_{19}S_4$	1702.64	1702.69	20.85	583	3.3 ± 1.2 (5)
14	SRBAC-ALALA-Tyr^3-octreotate	$C_{97}H_{129}N_{17}O_{23}S_4$	2028.84	2029.70	21.45	582	0.72 ± 0.08 (2)
15	SRBAC-Ahx-Lys(SRBAC)-Tyr^3-octreotate	$C_{115}H_{143}N_{17}O_{26}S_6$	2370.88	2371.09	22.65	583	51 ± 0 (2)
16	SR101AC-Ahx-Tyr^3-octreotate	$C_{86}H_{103}N_{13}O_{19}S_4$	1772.63 [M + Na$^+$]	1773.10	19.25	602	3.1 (1)

[a]For the conjugates **1**–**6**, the dye residue R101 carried a positive charge (counter ion: trifluoroacetate); for **7**–**16**, the dye was in a zwitterion form.
[b]Exact mass calculated for the measured positive ion: M^+ (**1**–**5**), [M^{+2}–H^+] (**6**), [M + H^+] (**7**–**15**), [M + Na^+] (**16**).
[c]*m/z* measured by precalibrated MALDI-TOF or ESI-MS (**1**–**6**, **10**–**16**) or by MALDI-TOF at low resolution (**7**–**9**).
[d]Retention time under RP-HPLC (see Experimental).

linkage site (Phe-NH-R) attacks C9 of the rhodamine core to form a five-membered ring with loss of a proton. As shown in Figure 6, C9 carries a partial positive charge due to the symmetric resonance structure shown. Other resonance structures distribute the positive charge onto the rhodamine nitrogens (Fig. 3). In the neutral lactam form large-scale electron delocalization would be eliminated with a concomitant loss of optical absorbance and fluorescence in the visible range. The amide-lactam equilibrium would be shifted toward the charged amide form at low pH, that is in the TFA-containing solvents used for isolation and purification.

The above hypothesis is supported by several recent studies (see Discussion), including the synthesis of analogous spirolactams from amine conjugates of fluorescein[19] and the investigation of Corrie et al.[20] of the amide-lactam equilibrium for an amine conjugate of rhodamine B and analogous ring closure equilibria for amine conjugates of sulforhodamine dyes containing a Phe-SO_2NHR moiety.

In order to provide NMR spectroscopic evidence for the amide-lactam equilibrium with our rhodamine 101 pep-

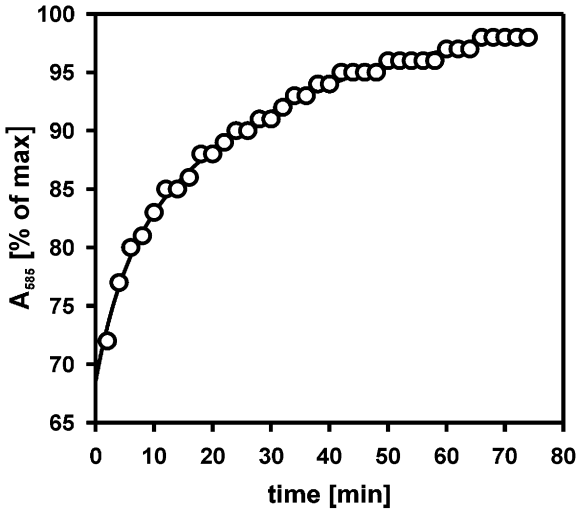

Figure 5. Time dependence of the optical absorbance (585 nm) of an aqueous solution of R101-Ahx-Tyr^3-octreotide (**1**) after a change in pH from 7.4 to 4.0. The increase in absorbance represents the conversion of the neutral, weakly absorbing spirolactam form of the rhodamine moiety to the positively charged open amide form.

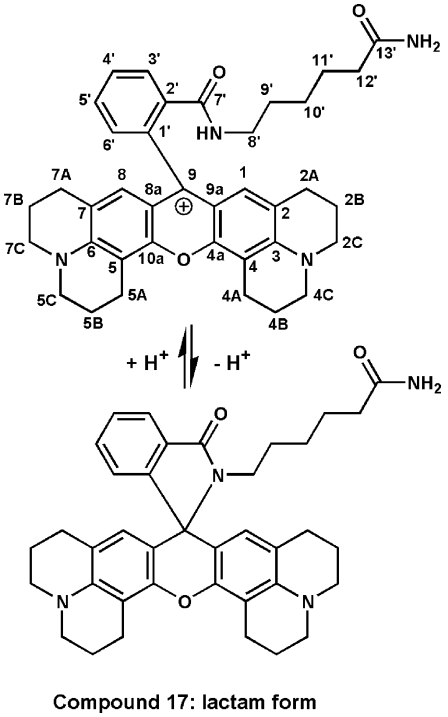

Figure 6. Structures of the amide and lactam forms of the model compound R101-Ahx-NH_2 (**17**) which exist in a pH-dependent equilibrium; the lactam is predominant at alkaline pH. The spirolactam ring is perpendicular to the rhodamine core; the overall symmetry is C_s. The numbering scheme is that used for NMR assignments.

tide–dye conjugates **1**–**6**, we synthesized by solid-phase chemistry the model compound **17** (Fig. 6), the amide conjugate of 6-amino-hexanoic acid with rhodamine 101 (R101-Ahx-NH_2). As isolated from TFA-containing solvent, **17** was completely characterized by high-field ^{1}H and ^{13}CNMR (Table 2). In CD_3OD solution the strongly absorbing and fluorescent amide form gave spectra closely resembling those obtained from rhodamine 101 (zwitterion) with additional signals from the Ahx unit. In particular, the ^{13}C resonances for C1′ and the neighboring C9 (partial positive charge) in **17** were observed at 133.33 and 156.44 ppm, respectively (R 101: 133.95, 160.73 pppm), while the singlet for the equivalent protons H1,8 (C_s symmetry) gave a chemical shift of 6.762 ppm (R101: 6.802 ppm).

Treatment of the NMR sample with borate–D_2O buffer at pH 11 led within 5 min to a loss of the deep violet color and partial precipitation. The poorly resolved ^{1}HNMR spectrum of the resulting slurry indicated that the H1,8 singlet had shifted upfield to ca. 5.9 ppm and that the methylene protons neighboring the rhodamine nitrogens (pos. 2C,7C and 4C,5C) had also shifted upfield, as expected for formation of a lactam with loss of the partial positive charge on the nitrogens of the rhodamine core. The slurry was extracted with $CDCl_3$, leading to a clear red, nonfluorescent solution in the organic phase. Complete analysis of the NMR spectra (Table 2) confirmed essentially quantitative conversion of the amide to the lactam form. In particular, the sp^3 carbon C9 now appeared at 66.55 ppm. Other key chemical shift changes are highlighted in bold face in Table 2 (see Discussion).

Discussion

Radiolabeled octreotide has been successfully used as a tumor-targeted diagnostic and radiotherapeutic due to its binding to SSTR, which are overexpressed by various tumors, especially of neuroendocrine origin. Neuroendocrine tumors tend to grow slowly and are notoriously difficult to localize, at least in early stages. Metastases are in most cases already present at the time of diagnosis. Surgery is the only curative therapeutic option, and effective treatment invariably requires the complete excision of all tumor tissue. Therefore, localization of primary tumors as well as metastases (pre- and intraoperatively) is of utmost importance. Microscopic and occult disease not readily seen by the surgeon may remain in situ, leading to a shortened survival period. On the other hand, the removal of large areas of noninfiltrated healthy tissue, especially in the brain, may cause severe side effects.

Thus, facilitated delineation of the resection margins is challenging. Previous experience with 5-ALA has proven the usefulness of tagging tissue with fluorescent markers in the intraoperative situation.[21–23] However, the selectivity of this process is limited by the auto-

Table 2. NMR data for the R101-Ahx-NH_2 conjugate **17** in amide and lactam forms[a]

Pos	^{13}C chem. shift and multiplicity		^{1}H chem. shift and multiplicity	
	Amide in CD_3OD	Lactam in $CDCl_3/CD_3OD$	Amide in CD_3OD[b]	Lactam in $CDCl_3/CD_3OD$[c]
1′	**133.33** S	**154.02** S		
2′	138.54 S	131.06 S		
3′	128.79 D	122.58 D	7.785 d	7.858
4′	131.53 D [d]	128.21 D	**7.714** dd	**7.454**
5′	131.05 D [d]	132.74 D	**7.714** dd	**7.457**
6′	131.65 D	124.16 D	**7.366** d	**7.078**
7′	170.03 S	168.93 S		
8′	40.47 T	40.24 T	3.062 t	3.076
9′	30.08 T	27.59 T	1.234 tt	1.120
10′	27.36 T	26.54 T	1.105 tt	1.119
11′	26.47 T	24.05 T	1.453 tt	1.429
12′	36.28 T	35.52 T	2.062 t	2.071
13′	178.74 S	177.57 S		
1,8	127.72 D	124.72 D	**6.762** s	**5.947**
2,7	125.16 S	117.60 S		
3,6	152.57 S	143.85 S		
4,5	106.62 S	108.11 S		
4a,10a	153.59 S	148.52 S		
8a,9a	114.38 S	105.73 S		
9	**156.44** S	**66.55** S		
2A,7A	28.60 T	27.30 T	2.719; 2.700	2.482
2B,7B	21.89 T	22.14 T	1.961; 1.957	1.871
2C,7C	**51.90** T	**50.11** T	**3.520**; **3.509**	**3.099**
4A,5A	21.01 T	21.36 T	3.071; 3.061	2.916
4B,5B	20.95 T	21.62 T	2.103; 2.093	2.057
4C,5C	**51.43** T	**49.68** T	**3.559**; **3.544**	**3.153**

[a]Determined at 500.13 MHz (^{1}H) and 125.76 MHz (^{13}C), 30 °C.
[b]Detailed analysis of second-order spin systems performed by iterative simulation (WIN-DAISY).
[c]Detailed analysis not performed; ^{1}H chem. shifts of CH_2 groups are the mean values for nearly equivalent protons, as determined by 2D CH correlation.
[d]Assignments for C4′, C5′ may be interchanged.

fluorescence of nontarget tissue. Several recent studies[24–26] describe fluorescent markers which are targeted to SSTR and which emit light in the invisible NIR region, requiring a sophisticated camera for visualization. Thus, there is a need for fluorescent markers which emit light in the visible spectrum, allowing a convenient interoperative visual detection of tumor tissue without additional equipment.

The blood chromophores and bilirubin determine dermal absorption at wavelengths longer than 320 nm, and scattering by collagen fibers largely determines the depths to which these wavelengths penetrate. Red dyes emit a more penetrating fluorescence than dyes such as fluorescein. An optical 'window' between 550 and 1300 nm, allows the use of long-wavelength fluorescent dyes for improved detection depth, and dyes which absorb and emit light in the visible part of this optical window (ca. 600 nm) are advantageous due to ease of visualization and low background.

Structure–activity relationships

Thus, the goal of the current study was to develop a synthesis protocol for preparing SSTR-targeted fluorescent dyes with the desired optical properties described above. As shown in Table 1, the fluorescent conjugates bind to rat cortex somatostatin receptors with relatively high affinity but with IC_{50} values which differ by up to two orders of magnitude. As a reference for comparisons, the IC_{50} for octreotide peptide alone was determined to be 2.8 nM in our competition assay utilizing ^{125}I-Tyr^3-octreotide, which has been reported to have high affinity ($K_D = 0.19$ nM) for the sst_2 subtype of SSTR.[27] The reported binding constants for octreotide ($pK_i = 9.8$) and somatostatin ($pK_i = 9.6$) to sst_2 are similar.[28] Consequently, the fluorescent conjugates with $IC_{50} < 10$ nM have the potential to compete with the endogenous peptide somatostatin in vivo.

The amino acid residues Phe^3(Tyr^3)-Trp^4-Lys^5-Thr^6 constitute the binding pharmacophor of somatostatin, octreotide, octreotate, and their derivatives. Modifications of this sequence have been reported to have a strong impact on the binding affinity of these peptides. Pairwise comparisons of the data in Table 1 indicate that conjugates with the Tyr^3 peptide have greater receptor affinities than the corresponding Phe^3 peptide conjugates (**5** vs **3**, **14** vs **12**). There is no significant difference in the affinities for octreotide conjugates versus the corresponding octreotate conjugates (**1** vs **4**, **7** vs **8**). The 10 'best' conjugates all include the Tyr^3-peptide unit.

Strong effects on binding due to N-terminal peptide modifications have been reported. For example, attachment of the metal chelator 1,4,7,10-tetraazacyclododecane-1,4,7,10-tetraacetic acid (DOTA) to the N-terminus of Tyr^3-octreotide strongly increased receptor affinity.[29] However, in the competitive binding assay for SSTR in human or rat cortex, Octreoscan (DTPA-octreotide) proved to be a weaker ligand than octreotide (pK_D reduced by ca. 0.8 units).[27] The two conjugates in the current study which lack a spacer moiety (**2**, **11**) exhibited the poorest binding ($IC_{50} = 58$ and 89 nM, respectively). Thus, without a spacer unit the dye moiety apparently prohibits an optimal interaction between peptide and receptor. The influence of the spacer's structure on binding appears to depend on the nature of the dye moiety. For R101 and RBITC conjugates the flexible Ahx spacer led to better binding than the bulkier ALALA spacer (**4** vs **5**, **8** vs **9**), while for the SRBAC dye the ALALA spacer proved to be advantageous (**13** vs **14**). The exceptionally good binding of **14**, the only conjugate with a K_D significantly lower than that for octreotide (0.72 vs 2.8 nM), is most likely due to specific favorable interactions between the spacer-dye moiety and the receptor surface adjacent to the peptide binding site. The use of the bifunctional spacer Ahx-Lys with two dye moieties led to only a minor reduction in affinity with R101 (**6** vs **4**) but a significant reduction with SRBAC (**15** vs **13**). Table 1 also offers comparisons in three groups of peptide–spacer–dye conjugates in which only the dye moiety was varied. In each case, the RBITC conjugates (**7**–**9**) proved to be significantly poorer ligands ($IC_{50} = 5.5$–27 nM), while the IC_{50} values for the other dye conjugates (**1**, **4**, **5**, **10**, **13**, **16**), with the exception of **14** (see above), all fell in the range 2.0–4.3 nM. Thus, compound **14** and the last-mentioned group of six compounds, which appear to bind to SSTR in an unhindered manner analogous to octreotide, represent the best choice of fluorescent peptide–dye conjugates for future in vivo testing. Although few publications have described the use of fluorescent dyes for the direct visualization of tumor tissue,[7,9] the improved SSTR targeting of the peptide–dye conjugates described here should result in more selective accumulation in tumor and improved potential for clinical applications.

Amide-lactam interconversion in rhodamine 101 conjugates

The R101 conjugates **1**–**6** were unique in their pH-dependent behavior. At pH >7 dye absorption and fluorescence were rapidly lost but were recovered when the pH was lowered to 4. The NMR data obtained from model compound **17** (R101–Ahx–NH_2) provide conclusive evidence for the formation of a spirolactam at alkaline pH. This intramolecular ring closure is exclusively possible in the R101 conjugates due to the amide functional group present at the *ortho* position C2′ (Fig. 6) when the dye is connected to any of the spacers used. Ring closure with loss of the positive charge on the rhodamine core leads to the disappearance of the sp^2 carbon signal for C9 at 156.44 ppm and the appearance of an sp^3 quaternary carbon signal at 66.55 ppm (predicted: 60.5). Analogous nonfluorescent spirolactams prepared from fluorescein exhibited C9 chemical shifts near 64 ppm.[19] The C1′ carbon of the benzamide group attached to C9 also shows a dramatic shift from 133.33 ppm in the amide to 154.02 ppm in the lactam. A similar effect has been documented for C1′ (132.0 to 153.2 ppm) for the conversion of a fluoran dye zwitterion (analogous to R101) to a spirolactone.[30] In addition, several other sp^2 carbon sites (C1,8; C2,7; C3,6; C4a,10a; C8a,9a) exhibited significant upfield shifts due to increased electron density, and the methylene carbons attached to the rhodamine nitrogens showed upfield

shifts of ^{1}H and ^{13}C signals, consistent with the loss of partial positive charge on nitrogen. The protons H1,8 are also sensitive to ring closure, exhibiting a shift from 6.762 to 5.947 ppm. A similar shift effect (6.75 to 6.12 ppm) has been observed for the corresponding protons in lissamine rhodamine sulfonamides which undergo analogous ring closure at alkaline pH.[31]

The pH-dependent amide–lactam equilibrium for R101 conjugates deserves further study since it is expected to have consequences for their use as fluorescent labels in vivo. At a pH in the range 7–7.4 (tumor cell cytosol) dye fluorescence will be weak due to the predominance of the lactam form. Only if SSTR-mediated uptake of the conjugate leads to accumulation in acidic lysosomal compartments, for example, is significant fluorescence expected. Thus, as proposed by Marchesini et al.[31] for rhodamine sulfonamides, the R101 conjugates may prove to be useful as indicators of an acidic environment with low background fluorescence from neutral environments.

Experimental

General

The peptides were analyzed and purified by liquid chromatography (HPLC) on a Gyncotech P-580 system (Germering, Germany) equipped with a variable SPD 6-A UV detector and a C-R5A integrator (both Shimadzu, Duisburg, Germany). The columns used were LiChrosorb® RP-select B (5 μm, 250×4 mm; 10 μm, 250×10 mm; Merck, Darmstadt, Germany). All analytical runs were performed with a linear gradient over 30 min of 5–95% acetonitrile in water (both solvents containing 0.1% TFA) at a flow rate of 0.7 mL/min. Unless otherwise stated, all preparative runs were performed with the same gradient and a flow rate of 4 mL/min. The peptides were synthesized manually with a home-built SPPS reactor. Lyophilization was performed on a Christ (Osterode, Germany) α1-2 lyophilizer. Membrane binding experiments were performed using a home-built filtration apparatus.

Mass spectrometry

Low-resolution mass spectrometric analysis (ca. ±2 m.u.) of the peptides and conjugates was performed on a matrix-assisted laser desorption ionization time-of-flight (MALDI-TOF) mass spectrometer (MALDI-1, Kratos Instruments, UK). Sample preparation was performed with a solution of 2′-(4-hydroxyphenylazo) benzoic acid in acetonitrile/water (1:1) containing 0.1% TFA. The matrix (0.6 μL) was placed on the target, followed by one drop (0.6 μL) of the analyte, and allowed to dry at room temperature. Analyses with higher resolution and absolute accuracy were obtained with a Reflex 3 MALDI-TOF (Bruker Daltonics) (accuracy: ca. ±0.5 m.u.) and confirmed with a Finnigan MAT TSQ-7000 triple-quadrupole mass spectrometer using electrospray ionization (ESI) in the positive-ion mode (accuracy: ca. ±0.4 m.u.).

Reagents

All standard synthesis reagents were purchased from Merck (Darmstadt, Germany). The chemicals for peptide synthesis were obtained from Novabiochem (Läufelingen, Switzerland). The fluorescent dyes and the reagents *N*-Fmoc-6-amino-hexanoic acid, thallium(III)trifluoroacetate, and triisoproplysilane (TIS) were obtained from Fluka (Buchs, Switzerland). Protein was determined using the Bradford assay kit (Sigma). Tyr^3-octreotide was prepared by SPPS (see below). The radioisotope $Na^{125}I$ was purchased from Amersham Pharmacia Biotech (Freiburg, Germany). ^{125}I-Tyr^3-octreotide was prepared by iodination of Tyr^3-octreotide using the chloramine-T method according to Bakker et al.[32] The product was purified by HPLC and stored at −80 °C until use.

Synthesis of peptides

Octreotate derivatives were assembled on Fmoc-Thr (^{t}Bu)-Wang resin, octreotide-derivatives on 4-(2′,4′-dimethoxyphenyl - Fmoc - aminomethyl) - phenoxy (Rink amide) resin. N^{α}-Fmoc amino acids with the following side chain protecting groups were employed: Cys-acetamidomethyl(Acm), Lys(Boc), Thr(^{t}Bu), Thr(ol)-terephthal-acetal[33] [used to attach Thr(ol) for the synthesis of the octreotide derivatives], D-Trp(Boc) and Tyr(^{t}Bu). The resin was swollen overnight in DCM and washed with DMF. A reaction cycle consisted of the following steps: (a) remove the current N-terminal Fmoc group by a short flow wash followed by shaking of the resin with piperidine/DMF (50:50, v/v) for 5 min, (b) preactivate a solution of 4 equiv of the Fmoc-protected monomer for 2 min in DMF with 3.9 equiv HBTU and 10 equiv DIPEA, (c) wash the resin with DMF (vacuum-assisted flow wash for 1 min), (d) perform the coupling reaction with the preactivated amino acid solution for 10 min, (e) wash the resin with DMF (vacuum-assisted flow wash 1 min). Instead of using repeated ninhydrin tests, an aliquot of the completed peptide was cleaved and analyzed by HPLC and MALDI-TOF-MS. The resin-bound peptides were cyclized with a 2-fold molar excess of $Tl(TFA)_3$ in DMF at room temperature. As determined by analysis of cleaved aliquots, formation of the disulfide bond was consistently complete within 1 h.

Conjugation of spacers and fluorescent dyes

Spacers were constructed from Fmoc-Lys(Fmoc)-OH, *N*-Fmoc-6-aminohexanoic acid, Fmoc-Ala-OH or Fmoc-Leu-OH. The conjugation of the spacers was performed as described for the amino acids of the peptide chain. Conjugation of rhodamine 101 was performed as for the extension of the peptide chain. For this purpose 4 equiv of the dye were preactivated for 10 min with 3.95 equiv HBTU and 10 equiv DIPEA in DMF. The activated dye was added to the swollen resin and shaken for 2 h. The conjugation reaction with sulforhodamine B acid chloride, sulforhodamine 101 or rhodamine B isothiocyanate was performed with 5 equiv of the dye using 10 equiv DIPEA. The dye was dissolved in DMF, added to the swollen resin and shaken. After 5 min, a solution

of DIPEA was added and the mixture was shaken overnight. The coupling efficiency was determined by HPLC and MALDI-TOF-MS analysis after cleavage of a small aliquot. When this analysis indicated completion of the conjugation reaction, the supernatant was removed. After thorough washings with DMF followed by DCM, the resin was shrunk in methanol and dried in vacuo overnight.

Cleavage and purification

The conjugates were cleaved by TFA/water/TIS (95/2.5/2.5) for 2 h. The conjugates were precipitated with diethyl ether. Excess TFA was removed by two precipitation/centrifugation steps. The precipitates were dissolved in water/acetonitrile (1:1) and purified by reversed-phase HPLC using 0.1% TFA in water and 0.1% TFA in acetonitrile as elution buffers. The products were isolated by RP-HPLC using the conditions described above and characterized by MALDI-TOF-MS. Based on the starting resin, the average yields of the purified products were approximately 40%. The conjugates synthesized and their properties are listed in Table 1.

Stability determination

Aliquots of the conjugates (final concentration = 10 μM) were incubated for up to 24 h at 37 °C with 200 μL of Soerensen buffer pH 7.4 or rat serum, both containing 5% DMF. After incubation, 1 volume of acetonitrile was added to each sample to stop the hydrolysis and to precipitate serum proteins. The samples were vortexed (30 s) and centrifuged (5 min at 13000 rpm). Subsequently, the supernatant was analyzed by HPLC. Separation of the intact peptide conjugate and the hydrolyzed fragments was carried out on a LiChrosorb® RP-select B column (5 μm, 250×4 mm). For comparison, the hydrolysis of somatostatin-14 in Soerensen buffer and rat serum was also examined.

Binding studies

The binding affinities of the peptide conjugates for somatostatin receptors in rat cortex membranes were determined by a competition assay employing ^{125}I-Tyr^3-octreotide, as described earlier.[34] Briefly, cortex membranes were suspended at a protein concentration of 500 μg/mL in 200 μL incubation buffer (100 μg protein per assay). The incubation buffer was 10 mM HEPES pH 7.6 containing 5% bovine serum albumin (BSA) fraction V, $MgCl_2$ (10 mM) and bacitracin (20 μg/mL). The cortex membranes suspension (200 μL) was mixed with 30 μL incubation buffer containing various concentrations of the competitor (10^{-10}–10^{-5} M of conjugates **1**–**16**). Approximately 20 pmol ^{125}I-Tyr^3-octreotide (ca. 20,000 cpm) in 70 μL incubation buffer were added. After 1 h at room temperature, the incubation was stopped by quick filtration through Whatman GF/B glass fiber filters prewetted with buffer containing 1% BSA. The filters were washed with ice-cold buffer (10 mM Tris, 150 mM NaCl, pH 7.6), and the bound radioactivity was counted in a gamma counter. Nonspecific binding, as determined by measuring binding in the presence of excess unlabeled octreotide (10 μM), was approximately 10–20% of the total binding. Specific binding was defined as total binding minus nonspecific binding. The results were expressed as the average specific binding obtained from multiple experiments.

9-[2-(5-Carbamoyl-pentylcarbamoyl)-phenyl]-2,3,6,7,12,13,16,17-octahydro-1*H*,5*H*,11*H*,15*H*-xantheno[2,3,4-*ij*:5,6,7-*i′j′*]diquinolizin-18-ium, inner salt (17). A 72 mg portion of Rink amide resin [4-(2′,4′-dimethoxyphenyl-Fmoc-aminomethyl)-phenoxy resin, 0.69 mmol/g resin] = 0.05 mmol was swollen in DCM over night. The Fmoc group was deprotected for 15 min with 50% piperidine/DMF, and the resin was washed thoroughly with DMF. In 1 mL DMF 70.6 mg *N*-Fmoc-6-amino-hexanoic-acid (4 equiv) and 72.4 mg HBTU (3.8 equiv) were dissolved and mixed with 100 μL DIPEA. After 2 min the mixture was added to the resin and shaken for 30 min. The Fmoc group was deprotected for 10 min with 50% piperidine/DMF, and the resin was washed thoroughly with DMF. In 1 mL DMF 49.1 mg of R101 (2 equiv) and 36.2 mg HBTU (1.9 equiv) were dissolved and mixed with 100 μL DIPEA. After 2 min, the mixture was added to the resin and shaken for 2 h. The resin was washed thoroughly with DMF followed by DCM and methanol. The product was cleaved with 1.0 mL TFA at room temperature for 60 min. The resin was removed by filtration and the TFA was concentrated to dryness. The crude product was taken up in a mixture of 500 μL H_2O and 500 μL acetonitrile and then purified by RP-HPLC on the RP-select B column (10 × 250 mm) with a linear gradient over 30 min of 0–80% acetonitrile in water (0.1% TFA in each solvent) at a flow rate of 0.7 mL/min. Under these conditions the product eluted at 25.1 min. Analytical runs were performed as described for the peptide conjugates. Under these conditions the product eluted at 23.97 min. ^{1}H and ^{13}C NMR data (CD_3OD) are presented in Table 2. For the molecular formula $C_{38}H_{43}N_4O_3^+$ the calculated exact mass is 603.3330; ESI-MS gave m/z = 603.45 for [M^+].

NMR spectroscopy: amide to lactam conversion of compound 17

^{1}H and ^{13}C NMR spectra of compound **17** were obtained at 11.7 T using a Bruker AM-500 spectrometer and a 5-mm ^{1}H/^{13}C dual probehead. The sample (ca. 10 mg as trifluoroacetate salt) was initially dissolved in 0.5 mL CD_3OD (99.96% D). A series of spectra was obtained for the positively charged amide form (Fig. 6), and signal assignments were made on the basis of H,H-COSY and CH 2D correlation experiments. Complete assignments for the parent compound, rhodamine 101, were obtained by analogous experiments, including long-range CH correlation via the COLOC-S experiment to unambiguously assign all quaternary carbons. These assignments were used to make the assignments for the quaternary carbons in **17** as listed in Table 2. Detailed analysis of the complex second-order ^{1}H NMR spectrum was performed using the simulation/iteration program WIN-DAISY (Bruker). This allowed the determination of the nonequivalent chemical shifts for the various pairs of methylene protons in the R101 ring system.

To the NMR sample of **17** (CD_3OD solution, dark violet in color) were added 0.15 mL of a 100 mM sodium borate buffer in D_2O at pH 11. Within a few min, the sample changed to a red-brown suspension. NMR measurements of this suspension gave spectra with rather broad resonances, but there was an indication that formation of the lactam had occurred (upfield shift of the singlet for H1,8). To this sample 0.4 mL $CDCl_3$ were added and the mixture was shaken for 5 min. This extraction procedure led to a clear red organic phase which contained **17** in essentially 100% lactam form, as determined by subsequent NMR measurements. The signal assignments in Table 2 were confirmed by H,H-COSY, CH correlation, COLOC-S long-range correlations, the ^{1}H-coupled ^{13}C spectrum, and selective ^{1}H-decoupling experiments. A detailed analysis of the ^{1}H spectrum with WIN-DAISY was not carried out for the lactam. The reported ^{1}H chemical shifts were derived from the CH correlation experiment, where for each of the rhodamine ring methylene groups, only a single ^{1}H shift was resolved, representing the mean value of the individual shifts for the nearly equivalent protons at each site.

Acknowledgements

The authors acknowledge funding from the 'Forschungs-Förderungsprogramm der Medizinischen Fakultät Heidelberg' AZ.: 335/1999. We would like to thank S. Fiedler and G. Erben of the German Cancer Research Center for recording MALDI-TOF and ESI mass spectra, respectively.

References and Notes

1. Nagakawa, T.; Nagamori, M.; Futakami, F.; Tsukioka, Y.; Kayahara, M.; Ohta, T.; Ueno, K.; Miyazaki, I. *Cancer* **1996**, *77*, 640.
2. Eker, C.; Montan, S.; Jaramillo, E.; Koizumi, K.; Rubio, C.; Andersson-Engels, S.; Svanberg, K.; Svanberg, S.; Slezak, P. *Gut* **1999**, *44*, 511.
3. Ladner, D. P.; Steiner, R. A.; Allemann, J.; Haller, U.; Walt, H. *Br. J. Cancer* **2001**, *84*, 33.
4. Carcenac, M.; Larroque, C.; Langlois, R.; van Lier, J. E.; Artus, J. C.; Pelegrin, A. *Photochem. Photobiol.* **1999**, *70*, 930.
5. Hasegawa, S.; Yang, M.; Chishima, T.; Miyagi, Y.; Shimada, H.; Moossa, A. R.; Hoffman, R. M. *Cancer Gene Ther.* **2000**, *7*, 1336.
6. Bornhop, D. J.; Hubbard, D. S.; Houlne, M. P.; Adair, C.; Kiefer, G. E.; Pence, B. C.; Morgan, D. L. *Anal. Chem.* **1999**, *71*, 2607.
7. Hamblin, M. R.; Rajadhyaksha, M.; Momma, T.; Soukos, N. S.; Hasan, T. *Br. J. Cancer* **1999**, *81*, 261.
8. Becker, A.; Riefke, B.; Ebert, B.; Sukowski, U.; Rinneberg, H.; Semmler, W.; Licha, K. *Photochem. Photobiol.* **2000**, *72*, 234.
9. Kremer, P.; Wunder, A.; Sinn, H.; Haase, T.; Rheinwald, M.; Zillmann, U.; Albert, F. K.; Kunze, S. *Neurol. Res.* **2000**, *22*, 481.
10. Hüber, M. M.; Staubli, A. B.; Kustedjo, K.; Gray, M. H.; Shih, J.; Fraser, S. E.; Jacobs, R. E.; Meade, T. J. *Bioconjug. Chem.* **1998**, *9*, 242.
11. Tung, C. H.; Mahmood, U.; Bredow, S.; Weissleder, R. *Cancer Res.* **2000**, *60*, 4953.
12. Krenning, E. P.; Kweekeboom, D. J.; Bakker, W. H.; Breemann, W. A. P.; Kooij, P. P. M.; Oei, H. Y.; van Hagen, M.; Postema, P. T. E.; de Jong, M.; Reubi, J. C.; Visser, T. J.; Reijs, A. E. M.; Hofland, L. J.; Koper, J. W.; Lamberts, S. W. J. *Eur. J. Nucl. Med.* **1993**, *20*, 716.
13. Bohuslavizki, K. H. *J. Nucl. Med.* **2001**, *42*, 1057.
14. Henze, M.; Schuhmacher, J.; Hipp, P.; Kowalski, J.; Becker, D. W.; Doll, J.; Maecke, H. R.; Hofmann, M.; Debus, J.; Haberkorn, U. *J. Nucl. Med.* **2001**, *42*, 1053.
15. Trouet, A.; Masquelier, M.; Baurain, R.; Deprez-De Campeneere, D. *Proc. Natl. Acad. Sci. U.S.A.* **1982**, *79*, 626.
16. Patel, Y. C. *Front. Neuroendocrinol.* **1999**, *20*, 157.
17. Czerwinski, G.; Tarasova, N.; Michejda, C. J. *Proc. Natl. Acad. Sci. U.S.A.* **1998**, *95*, 11520.
18. Schoeffter, P.; Perez, J.; Langenegger, D.; Schupbach, E.; Bobirnac, I.; Lubbert, H.; Bruns, C.; Hoyer, D. *Eur. J. Pharmacol.* **1995**, *289*, 163.
19. Adamczyk, M.; Grote, J. *Tetrahedron Lett.* **2000**, *41*, 807.
20. Corrie, J. E. T.; Davis, C. T.; Eccleston, J. F. *Bioconjug. Chem.* **2001**, *12*, 186.
21. Kriegmair, M.; Zaak, D.; Knuechel, R.; Baumgartner, R.; Hofstetter, A. *Urol. Int.* **1999**, *63*, 27.
22. Malik, E.; Berg, C.; Meyhofer-Malik, A.; Buchweitz, O.; Moubayed, P.; Diedrich, K. *Surg. Endosc.* **2000**, *14*, 452.
23. Gahlen, J.; Stern, J.; Laubach, H. H.; Pietschmann, M.; Herfarth, C. *Surgery* **1999**, *126*, 469.
24. Achilefu, S.; Dorshow, R. B.; Bugaj, J. E.; Rajagopalan, R. *Invest. Radiol.* **2000**, *35*, 479.
25. Licha, K.; Hessenius, C.; Becker, A.; Henklein, P.; Bauer, M.; Wisniewski, S.; Wiedenmann, B.; Semmler, W. *Bioconjug. Chem.* **2001**, *12*, 44.
26. Becker, A.; Hessenius, C.; Licha, K.; Ebert, B.; Sukowski, U.; Semmler, W.; Wiedenmann, B.; Grotzinger, C. *Nat. Biotechnol.* **2001**, *19*, 327.
27. Piwko, C.; Thoss, V. S.; Schüpbach, E.; Kummer, J.; Langenegger, D.; Probst, A.; Hoyer, D. *Naunyn-Schmiedeberg's Arch. Pharmocol.* **1997**, *355*, 161.
28. Stolz, B.; Smith-Jones, P.; Albert, R.; Tolcsvai, L.; Briner, U.; Ruser, G.; Mäcke, H.; Weckbecker, G.; Bruns, C. *Digestion* **1996**, *57(Suppl. 1)*, 17.
29. Heppeler, A.; Froidevaux, S.; Mäcke, H. R.; Jermann, E.; Behe, M.; Powell, P.; Hennig, M. *Chem. Eur. J.* **1999**, *5*, 1974.
30. Yanagita, M.; Aoki, I.; Tokita, S. *Bull. Chem. Soc. Jpn.* **1997**, *76*, 2757.
31. Marchesini, S.; Gatt, S.; Agmon, V.; Giudici, M. L.; Monti, E. *Biochem. Int.* **1992**, *27*, 545.
32. Bakker, W. H.; Krenning, E. P.; Breeman, W. A.; Koper, J. W.; Kooij, P. P.; Reubi, J. C.; Klijn, J. G.; Visser, T. J.; Docter, R.; Lamberts, S. W. *J. Nucl. Med.* **1990**, *9*, 1501.
33. Hsieh, H. P.; Wu, Y. T.; Chen, S. T.; Wang, K. T. *Bioorg. Med. Chem.* **1999**, *7*, 1797.
34. Mier, W.; Eritja, R.; Mohammed, A.; Haberkorn, U.; Eisenhut, M. *Bioconjug. Chem.* **2000**, *11*, 855.